Organic Electrode Materials and Carbon/Small-Sulfur Composites for Affordable, Lightweight and Sustainable Batteries

SCHOLARONE™
Manuscripts

Organic Electrode Materials and Carbon/Small-Sulfur Composites for Affordable, Lightweight and Sustainable Batteries

Chao Luo*[a,b]

Redox-active organic/polymeric materials and carbon/small-sulfur composites are promising electrode materials for developing affordable, lightweight, and sustainable batteries because of their low cost, abundance, low carbon footprint, and flexible structural tunability. This feature article summarized the key aspects of the research related to organic batteries and Li-S batteries (LSBs) based on organic/polymeric/sulfur materials for next-generation sustainable energy storage. An in-depth discussion for organic electrode materials in alkali-ion, multivalent metal, all-solid-state, and redox flow batteries is provided. State-of-the-art LSBs under high mass loading and lean electrolyte conditions for practical applications is also covered. The challenges, reaction mechanisms, strategies, approaches, and developments of organic batteries and LSBs are discussed to offer guidance for rational structure design and performance optimization. This feature article will contribute to the development and commercialization of affordable, lightweight, and sustainable batteries.

Introduction

Due to excessive utilization of fossil fuels in the last two centuries, climate change becomes a critical challenge for the sustainable development of human society. To address this challenge, developing alternative energy supply resources based on clean energy and carbon neutrality is vital.[1,2] To fulfill this goal, significant progress has been made for energy harvesting technologies to effectively utilize renewable energies such as solar energy, wind power, etc.[3-5] However, the intrinsic intermittent nature and uneven geological distribution of renewable energies require efficient energy storage devices to store and distribute these clean energies. So far, rechargeable lithium batteries, which are dominant energy storage devices for portable electronics and electric vehicles, are also used to store renewable energies.[6,7] Nevertheless, high cost, high toxicity, and scarcity of heavy transition metals in commercial lithium batteries impede the large-scale application.[8,9] It is essential to exploit transition metal-free electrode materials as alternatives to achieve affordable, lightweight, and sustainable batteries.

Among emerging materials for rechargeable batteries, redox-active organics, polymers, and sulfur materials, consisting of light elements such as C, H, O, N, and S, stand out because of low cost, abundance, lightweight, recyclability, degradability, sustainability, abundant structure diversity, and flexible structure tunability.[10-15] More importantly, organic electrode materials (OEMs) and sulfur have been demonstrated to be universal materials in various rechargeable batteries such as non-aqueous Alkali (Li/Na/K) ion

batteries, multivalent metal batteries, all-solid-state batteries, aqueous batteries, dual-ion batteries, and redox-flow batteries.[16-30] The unique physicochemical properties endow these sustainable materials with great promise for cost-effective, lightweight, and sustainable batteries. Moreover, they can also be used under extreme conditions such as fast charge/discharge and a wide temperature range, demonstrating promising electrode materials in batteries for electric vehicles and grid-scale energy storage.[31-35]

Though OEMs and sulfur are promising materials for sustainable batteries, there are three challenges that hinder their development:[36-49] 1) Low conductivity. Most organics, polymers, and sulfur suffer from low electronic conductivity, which limits the reaction kinetics. The addition of a large amount of conductive carbon in the electrodes enhances the conductivity at the price of decreasing the overall capacity and energy density of the batteries. 2) High solubility in the electrolytes. Due to the dissolution of pristine materials and/or reaction intermediates/products in the electrolytes, organic/polymeric/sulfur electrodes suffer from capacity decay upon long-term cycling, leading to poor cycle life. 3) Large volume change. Volume expansion and shrinkage caused by ion insertion/extraction during battery charge and discharge compromise structure integrity and induce particle pulverization, leading to fast capacity fading upon cycling. To overcome these challenges, various strategies using different types of conductive carbons, ionic bonding, polymerization, high concentration electrolytes, etc. were employed.[50-59] This feature article summarized the research work for addressing these challenges in organic batteries and Li-S batteries (LSBs).

The discussions are focused on two directions to achieve affordable, lightweight, and sustainable energy storage: 1) OEMs for affordable and sustainable organic batteries; 2) Carbon/small-sulfur

a. Department of Chemistry and Biochemistry, George Mason University, Fairfax, VA, 22030, USA.
b. Quantum Science & Engineering Center, George Mason University, Fairfax, VA, 22030, USA.

composites for high-energy and sustainable LSBs. OEMs are redox-active small organic molecules and polymers that contain functional groups such as carbonyl, imine, azo, amine, and disulfide groups, nitroxide free radicals, etc.[60,61] These functional groups can reversibly react with cations or anions in the batteries. As shown in figure 1a, Luo et al. started to work in this field over a decade ago and reported a variety of carbonyl-based organic anode and cathode materials for Li-ion and Na-ion batteries.[62-70] In 2018, azo chemistry was introduced into the battery field by Luo et al. Several azo compounds were applied in Li-ion, Na-ion, K-ion, and all-solid-state batteries and demonstrated superior electrochemical performances in terms of high capacity, long cycle life, and fast reaction kinetics.[71-75] Since 2019, Luo et al. have reported various linear and porous polymers as cathode materials for alkali-ion and multivalent metal batteries.[76-81] The results illustrate that developing organic salts and high-molecular-weight polymers can effectively overcome the high solubility challenge of organic batteries. Extended conjugation structures in OEMs enhance reaction kinetics and enable fast charging capability.

Similar challenges such as sluggish reaction kinetics and shuttle reactions also present in LSBs due to low conductivity of sulfur and lithium sulfide, as well as high solubility of high-order polysulfide intermediates. To circumvent these challenges, a rich variety of host materials such as porous carbons, graphene, carbon nanotubes, conductive polymers, etc. were designed to enhance the conductivity of the sulfur cathode and trap polysulfides in the cathode.[82,83] However, the dissolution of polysulfides is still inevitable because of poor kinetics of sulfur and corresponding intermediates/products during the lithiation/de-lithiation process in the solid state. The dissolution of polysulfides in the organic electrolytes enables the fast liquid-phase reaction in LSBs.[84] This process will consume the electrolyte, so flooded electrolytes are used for S_8-based cathodes. To fulfill practical applications, the lean-electrolyte condition with a low electrolyte to sulfur ratio is requested. To this end, small sulfur molecules ($S_{2\sim3}$) were synthesized by co-annealing nature sulfur (S_8) with organic/polymeric carbon precursors.[85] Small sulfur molecules can be converted to insoluble Li_2S_2 and Li_2S without forming high-order polysulfides, preventing shuttle reactions. The uniform distribution of small sulfur molecules in the carbon matrix endows carbon/small sulfur composites with high conductivity and stability. In addition to sulfur, other chalcogens such as selenium and selenium sulfides with higher conductivity were also studied to achieve high sustainability and high energy density batteries.[86-90] The second research direction is shown in figure 1b. This feature article is focused on these two research directions, aiming to develop low-cost and sustainable organic/polymeric/sulfur materials to achieve affordable, lightweight, and sustainable batteries.

Organic Batteries

Organic batteries are sustainable energy storage devices based on affordable, lightweight, abundant, recyclable, and degradable OEMs. However, the challenges of low conductivity, high solubility, and particle pulverization of OEMs impede the development and commercialization of organic batteries. This section discusses the
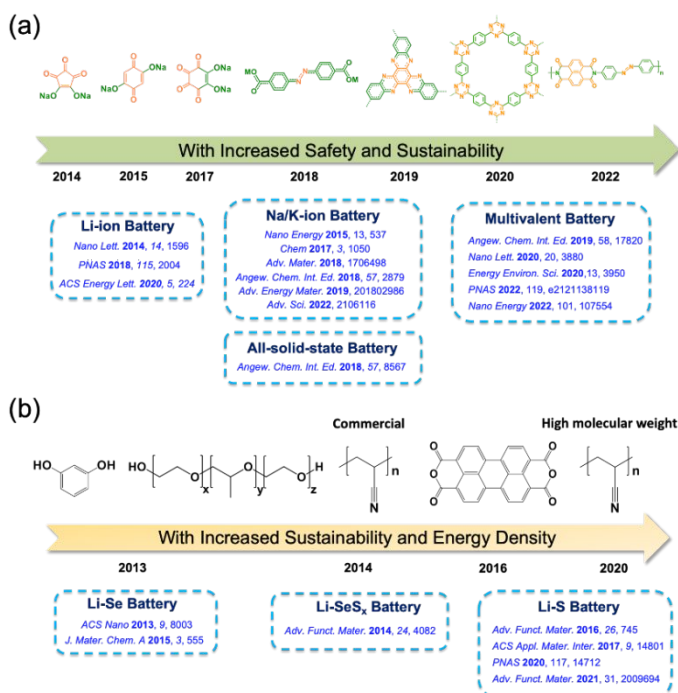

Fig. 1 Two research directions for affordable, lightweight, and sustainable batteries. (a) Organic batteries based on various organic and polymeric cathode and anode materials; (b) Li-Se/SeS$_x$/S batteries based on different carbon precursors.

approaches to addressing these challenges, as well as the performances and applications of OEMs in various rechargeable batteries.

OEMs suffer from low electronic conductivity, so a large amount ($\geq$ 30wt%) of conductive carbon such as carbon black is usually added in organic electrodes to enhance the electrode conductivity. Other highly conductive carbons such as graphene, carbon nanotubes, porous carbons, etc. are also widely used in organic electrodes.[91,92] The use of these carbons in organic electrodes increase electronic conductivity and reaction kinetics but lowers the energy density of organic batteries. In addition to low conductivity, high solubility and particle pulverization challenges also compromise the electrochemical performance of organic batteries.[93] To circumvent all the these challenges, Luo et al. designed and synthesized organic nanowires of croconic acid disodium salt (CADS) using an antisolvent crystallization method.[62] Reducing the particle size of CADS from microscale to nanoscale can effectively mitigate the volume change induced particle pulverization and enlarge the surface area to enable better contact between the organic active material and conductive carbon. 20 wt% carbon is used in the CADS electrode. Moreover, salt formation introduces ionic bonding between Na ion and O to enhance the polarity and reduce the solubility. Hence, a high-performance organic electrode based on CADS nanowires was reported in Li-ion batteries (LIBs). As shown in figure 2a, the nanowire structure can minimize the volume change and thus retain the structure integrity during lithiation and de-lithiation, while the microwire structure suffers from particle pulverization and poor structure integrity. Moreover, an ion exchange process was discovered that Na ions in CADS were replaced by Li ions after cycling. Figure 2b shows the nanowire structure of

ARTICLE

CADS. Compared with CADS microwires and micropillars, CADS nanowires exhibited significantly improved battery performances in terms of higher specific capacity, better cycle life, and faster reaction kinetics (Fig. 2c-e). This result proves that the developing nanostructured organic salts is an effective approach to addressing the challenges in organic batteries.
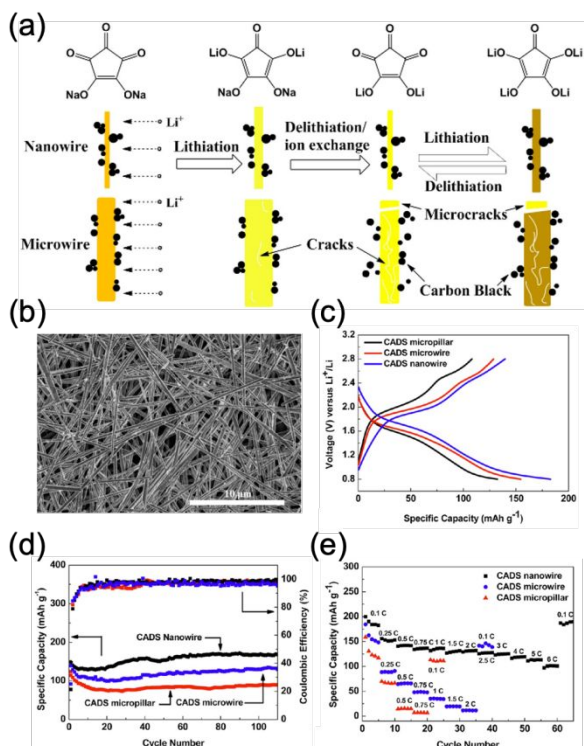

Fig. 2. Organic nanowires based on croconic acid disodium salt (CADS) for LIBs. (a) Schematic illustration for the volume change and ion exchange during lithiation and delithiation; (b) SEM image of CADS nanowires; Charge and discharge curves (c), cycle life (d), and rate capability (e) of CADS micropillar, microwire, and nanowire. Reproduced from reference 62 with permission from American Chemical Society, Copyright 2014.

Based on this result, organic salts with reduced particle sizes were also developed for Na-ion batteries (NIBs), which is more challenging than LIBs due to the larger ion size of Na ion than Li ion. Using the same organic salt (CADS), Luo et al. synthesized sub-micrometer size CADS and graphene oxide wrapped CADS using an aerosol spray technique to increase conductivity of the organic electrode, decrease the solubility of the organic active material, and prevent particle pulverization.[63] As shown in figure 3a, carbonyl groups in CADS can reversibly react with two Na ions and two electrons, accompanied by the intramolecular electron transfer in the conjugated structure. The schematic illustration for pristine CADS, sub-micrometer size CADS, and graphene oxide wrapped CADS is shown in figure 3b. As expected, graphene oxide wrapped CADS with a small particle size and high conductivity exhibited the highest capacity and longest cycle life among the three CADS electrodes, confirming that reducing particle size of organic salts is an effective approach to improving the performance of organic batteries. In addition to CADS, another organic salt named 2,5-Dihydroxy-1,4-

benzoquinone disodium salt (DHBQDS) is used to synthesize organic nanorods for high-performance NIBs.[64] The molecular structure and reaction mechanism of DHBQDS are shown in figure 3c. This work not only studied the nanostructure but also exploited the impacts of the binder, the fluorinated electrolyte, and atomic layer deposition (ALD) to the electrochemical performance. Figures 3d-g show the galvanostatic charge-discharge behaviors and long-term cycle life of DHBQDS electrodes in NIBs. The result indicates that the combination of the sodium alginate (SA) binder, the fluoroethylene carbonate-based electrolyte, and 1~2nm Al_2O_3 layer on the DHBQDS electrode by ALD can improve cyclic stability in NIBs and retain the high specific capacity. Apart from the nanostructure, the binder, the electrolyte, and the interphase play crucial roles in the electrochemical performance of organic batteries.
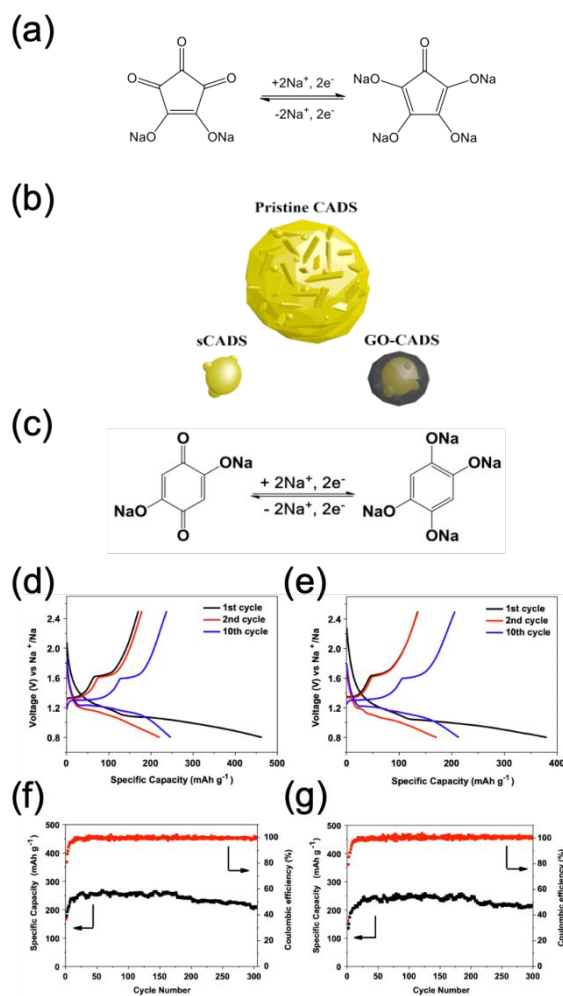

Fig. 3. Carbonyl-based organic salts for NIBs. (a) Reaction mechanism of CADS; (b) Schematic illustration of pristine, submicrometer-size, and graphene oxide wrapped CADS; Reproduced from reference 63 with permission from Elsevier B.V., Copyright 2014. (c) Reaction mechanism of 2,5-Dihydroxy-1,4-benzoquinone disodium salt (DHBQDS); The galvanostatic charge–discharge curves of the DHBQDS nanorod electrode covered with 1 nm Al_2O_3 layer (d) and 2 nm Al_2O_3 layer (e) with sodium alginate binder in $NaClO_4$-FEC/DMC electrolyte at the current density of 50 mA g^{-1}; desodiation capacity and Coulombic efficiency of DHBQDS nanorod electrode covered

with 1 nm Al_2O_3 layer (f) and 2 nm Al_2O_3 layer (g). Reproduced from reference 64 with permission from Elsevier B.V., Copyright 2015.

To further mitigate particle pulverization and improve the integrity of organic electrodes, self-healing chemistry between a redox-active organic salt (sodium rhodizonate dibasic, SRD) and the SA binder was exploited.[65] As shown in figure 4a, the two carbonyl groups can reversibly react with two Na ions and two electrons in NIBs, accompanied by intramolecular electron transfer in the conjugated structure. Hydrogen bonding (Fig. 4b) between oxygen in SRD and the hydroxyl group in SA self-heals the cracks and pulverization in organic electrodes upon cycling. The hydrogen bond is confirmed by Fourier transform infrared spectroscopy (FTIR) in figure 4c. For the SA binder, the deformation peak of pyranose rings at ~1,300 cm^{-1} disappears due to hydrogen bonding between SRD and SA. The SRD-SA electrode showed reversible redox plateaus in NIBs (Fig. 4d). To verify the role of self-healing chemistry, a control SRD electrode with the polyvinylidene fluoride more commonly (PVDF) binder was prepared. The SRD-SA electrode outperforms the SRD-PVDF electrode in terms of cyclic stability and rate capability (Fig. 4e and 4f). Various techniques such as SEM, Raman spectroscopy, and electrochemical impedance spectroscopy (EIS) were employed to confirm the self-healing chemistry in the SRD-SA electrode to heal the cracks and pulverizations. This work offers a new approach to addressing the challenges in organic batteries.
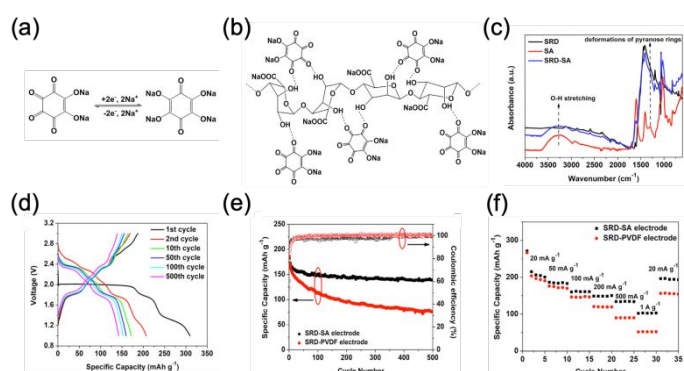

Fig. 4. The Reaction Mechanism and Self-Healing Chemistry of the SRD Electrode. (a) The sodiation-desodiation mechanism for SRD; (b) Schematic illustration of hydrogen bonding between SRD and SA; (c) FTIR spectra for SRD, SA, and the SRD-SA electrode; (d) The galvanostatic charge-discharge curves of the SRD- SA electrode; (e) Cycle life of the SRD-PVDF and SRD-SA electrodes at a current density of 50 mA g^{-1}; (f) Rate capability of the SRD-SA and SRD-PVDF electrodes. Reproduced from reference 65 with permission from Elsevier B.V., Copyright 2017.

Since carbonyl-based organic salts exhibited superior electrochemical performance in LIBs and NIBs, they are further applied in rechargeable potassium batteries. A fast-charging and high-temperature all-organic potassium battery based on a tetrahydroxy-1,4-benzoquinone potassium salt/N-doped graphene (TBPS/NG) as an anode and polyaniline/N-doped graphene (PANI/NG) as a cathode was achieved and delivered high performance in a wide temperature range from room temperature to high temperature up to 100^oC (Fig. 5a).[94] The reaction mechanisms

in the anode and cathode of the battery are shown in figure 5b. The n-type organic anode, TBPS, reversibly reacts with K ions and electrons, while the p-type polymer cathode, PANI, reversibly reacts with PF_6^- anions and electrons. The all-organic batteries with high anode mass loading of 6.5 mg cm^{-2} exhibit a long cycle life of 1,000 cycles and fast-charge capability up to 2 A g^{-1} at the room temperature (Fig. 5c). More importantly, with a high-concentration electrolyte of KPF_6 in diglyme (DEGDME), the all-organic batteries can deliver excellent cyclic stability of 300 cycles and fast-charge capability up to 2 A g^{-1} at the high operating temperatures up to 100^oC (Fig. 5d). Therefore, OEMs can be used under extreme conditions for fast-charging and high-temperature battery applications. More research efforts should be devoted to developing organic batteries with high performances and high energy density in a wide temperature range and fast-charging capability.
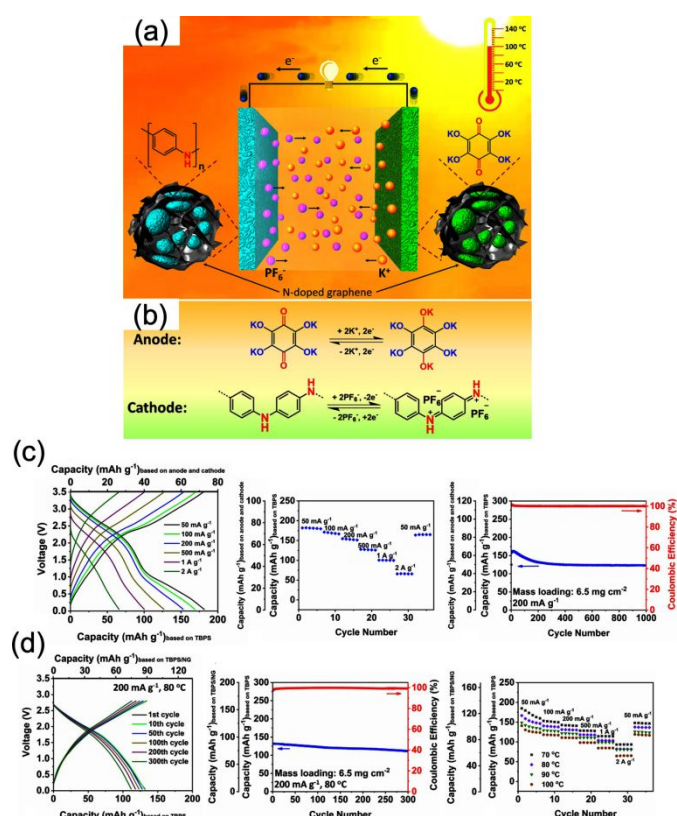

Fig. 5. All-organic K batteries. (a) The schematic of the all-organic rechargeable potassium battery; (b) Redox reactions in the organic anode and cathode during charge/discharge; (c) Charge/discharge curves at different C-rates, rate performance at various current densities, and discharge capacities and Coulombic efficiency measured at 200 mA g^{-1}; (d) charge/discharge curves, cycling stability of the all-organic RPB at 80 °C under the current density of 200 mA g^{-1}, and rate capability of the all-organic RPB at high temperatures. Reproduced from reference 94 with permission from Wiley-VCH Verlag GmbH & Co. KGaA, Copyright 2022.

To ultimately solve the challenges of organic batteries, it is of great importance to explore new chemistries for OEMs. Since electrochemical reactions of OEMs in organic batteries are based on various functional groups, the studies of the reactivity of functional

groups and corresponding reaction intermediates and products are critical. As shown in figure 6, there are several conventional reactions in organic batteries, which are disulfide, doping, carbonyl, and imine reactions based on disulfide, nitroxide free radical, carbonyl, and imine groups, respectively.[75] Luo et al. investigated the redox reaction of nitro groups in LIBs and discovered that the nitro group can be irreversibly reduced by Li ions and electrons to form nitroso group, azoxy group, and azo group. The azo group can reversibly react with Li ions and electrons in LIBs. The discovery of azo chemistry in rechargeable batteries offer better structural design flexibility for OEMs.
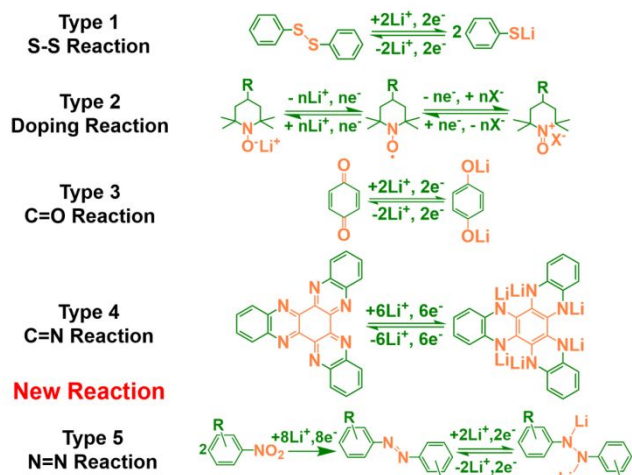

Fig. 6. Working principles of organic molecules in Li-ion batteries. In N=N reaction, two nitro groups are reduced to an azo group by Li-ions, with the formation of Li_2O. Reproduced from reference 75 with permission from Wiley-VCH Verlag GmbH & Co. KGaA, Copyright 2018.

To understand the performances and reaction mechanisms of azo compounds in rechargeable batteries, azo benzene (AB) and its derivatives were employed and applied in LIBs, NIBs, K-ion batteries (KIBs), and all-solid-state batteries. As shown in figure 7a, three azo compounds, AB, methyl red sodium salt (MRSS), and azobenzene-4,4'-dicarboxylic acid lithium salt (ADALS), were studied as electrode materials in LIBs.[71] The azo functional group can react with two Li ions and two electrons to reduce the nitrogen-nitrogen double bond to the nitrogen-nitrogen single bond (Fig. 7b). This electrochemical reaction is highly reversible. However, AB and MRSS are soluble in the organic electrolytes, resulting in fast capacity loss upon cycling. To overcome this challenge, two lithium carboxylate groups were introduced into AB to form ADALS with ionic bonding. The enhanced polarity significantly reduces the solubility in the electrolytes, and the solubility of ADALS in the carbonate-based commercial electrolyte is negligible. Thus, superior electrochemical performances have been achieved for ADALS in LIBs. As shown in figures 7c-h, ADALS exhibits two pairs of redox plateaus centered at ~1.5V with very small potential hysteresis. A specific capacity of ~190 mAh g^{-1} at a low current density of 0.5C can be retained for 100 cycles. When increasing the current density to 2C, 10C, and 20C, the reversible capacity is still retained at above 100 mAh g^{-1},

demonstrating robust reaction kinetics and fast charging capability. This result confirms that introducing carboxylate groups in azo compounds can significantly decrease the solubility in the electrolyte and improve the electrochemical performance. Carboxylated azo compounds are promising electrode materials for LIBs.
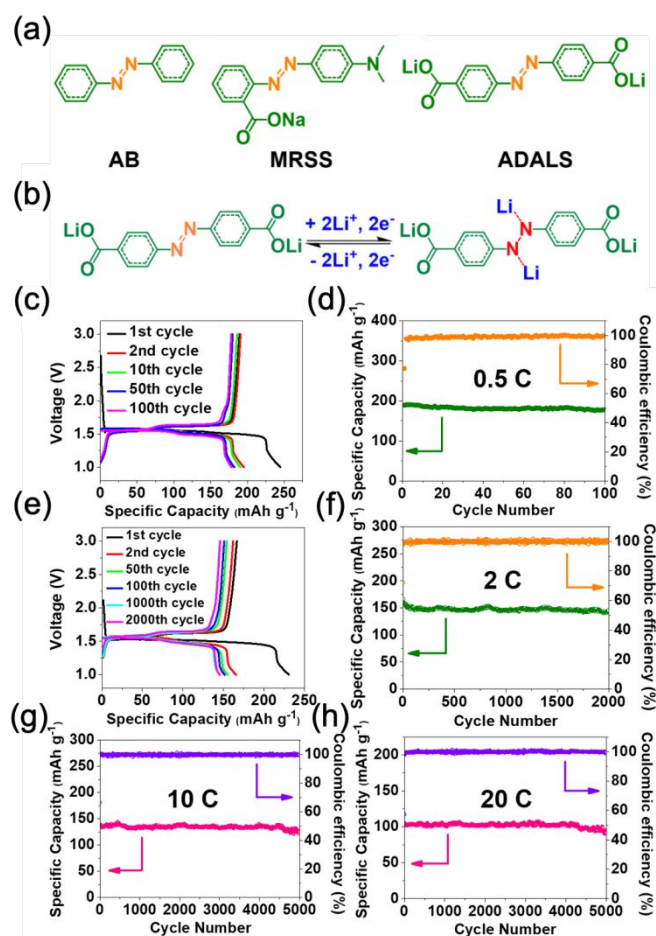

Figure 7. Azo compounds for LIBs.[71] (a) Molecular structure of AB, MRSS, and ADALS; (b) Reaction mechanism for ADALS; (c) The galvanostatic charge–discharge curves at 0.5 C; (d) Delithiation capacity and Coulombic efficiency versus cycle number at the current density of 0.5 C; (e) The galvanostatic charge–discharge curves at 2 C; Delithiation capacity and Coulombic efficiency versus cycle number at 2 C (f), 10 C (g), and 20 C (h).

In addition to LIBs, azo compounds are also applicable to other types of rechargeable batteries such as all-solid-state batteries, NIBs, and KIBs. Among various rechargeable batteries, applying OEMs in all-solid-state batteries is a promising research direction, because it ultimately addresses the high solubility challenge of organic batteries (Fig. 8a).[74] Two azo compounds, AB and 4-(phenylazo) benzoic acid lithium salt (PBALS), were used in nonflammable sulfide-based all-solid-state lithium batteries. It was found that the lithium carboxylate group in PBALS can interact with the Li_3PS_4 (LPS) solid electrolyte via the ionic bonding between oxygen in PBALS and lithium ion in LPS. This interaction stabilizes the contact interface by enabling intimate contact for the triple phase of the active material, the LPS solid electrolyte, and carbon in the all-solid-state batteries, so the electrochemical performances of PBALS outperform that of AB

without the lithium carboxylate group. A stable all-solid-state lithium organic battery was achieved by coupling a carboxylate azo compound with the LPS solid electrolyte.

Since carboxylated azo compounds show exceptional performances in LIBs and all-solid-state lithium batteries, they were further studied in NIBs and KIBs.[72,73] Similar to that in LIBs, the azo group can also reversibly react with Na ions and electrons in NIBs (Fig. 8b). The carboxylated azo compound delivers a pair of redox plateaus at ~1.3V with a reversible capacity of ~170 mAh g^{-1}. Excellent cyclic stability of up to 2,000 cycles was achieved at the current densities of 0.2C, 10C, and 20C (Fig. 8c-f), demonstrating ultra-stable and fast-charging batteries. The high performances of carboxylated azo compounds are also extended to KIBs. Liang et al. reported the azobenzene-4,4'-dicarboxylic acid potassium salt as a promising organic anode material for high-temperature KIBs.[73] These results confirm that azo compounds are universal electrode materials for various rechargeable batteries with high capacity, long cycle life, and fast charging capability.

capacity and Coulombic efficiency versus cycle number at 10C (e) and 20C (f). Reproduced from reference 72 with permission from Wiley-VCH Verlag GmbH & Co. KGaA, Copyright 2018.

In addition to salt formation, another strategy to address the high-solubility challenge of organic batteries is developing redox-active polymers. As well-documented, the solubility of organic materials is decreased with the increase of the molecular weight. Increasing the molecular weight of OEMs to form redox-active polymers offers insoluble OEMs for various organic batteries. For example, a pyrazine-based two-dimensional polymer in figure 9a can reversibly react with Na ions and electrons to reduce the C=N groups and trigger intramolecular electron transfer in NIBs.[76] Exceptional electrochemical performance is achieved because of the insolubility of the polymer and its intermediates/product during battery charge and discharge, as well as the high porosity, which enables fast reaction kinetics. The pyrazine-based polymer delivers slopping redox plateaus centered at ~2V with a reversible capacity over 200 mAh g^{-1} and a long cycle life over 100 cycles (Fig. 9b-c). Due to the high performance in NIBs, the polymer is further applied in multivalent batteries such as rechargeable Mg/Al batteries. The reversible capacity of over 100 mAh g^{-1} is still retained in multivalent batteries (Fig. 9d-e), and high cyclic stability of 200 cycles and 100 cycles is achieved in pouch cells for rechargeable Mg and Al batteries, respectively (Fig. 9f-g), demonstrating a universal polymer cathode for high-stability and fast-charging batteries.
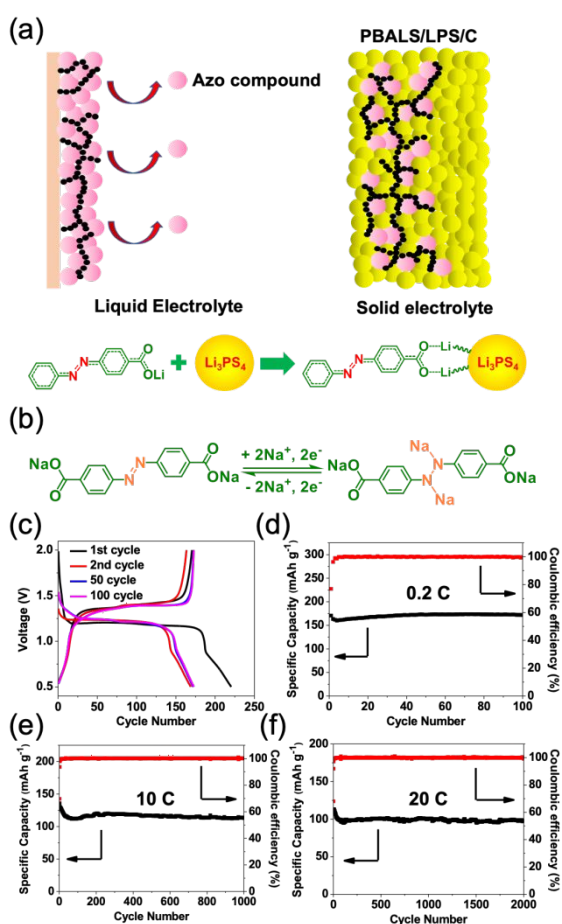

Fig. 8. Azo compounds in all-solid-state batteries and NIBs. (a) Schematic illustration for AB/PBALS in liquid and solid electrolytes, as well as the interaction between PBALS and LPS solid electrolyte; Reproduced from reference 74 with permission from Wiley-VCH Verlag GmbH & Co. KGaA, Copyright 2018. (b) The reaction mechanism of ADASS in NIBs; (c) The galvanostatic charge–discharge curves at 0.2C; (d) De-sodiation capacity and Coulombic efficiency versus cycle number at the current density of 0.2C; De-sodiation
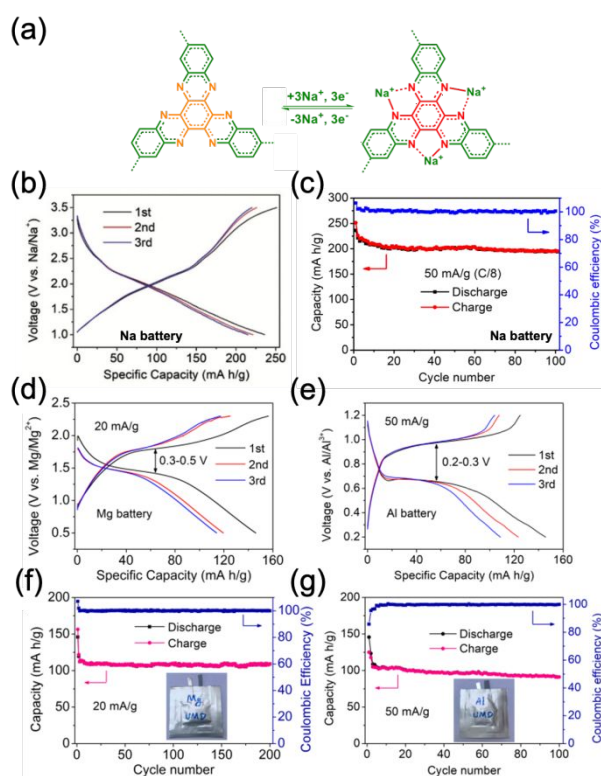

Fig. 9. A pyrazine-based polymer for fast-charge batteries. (a) The reaction mechanism; (b) Discharge-charge curves of PHATN at 50 mA g^{-1} in NIBs; (c) Cycle life in NIBs; Discharge-charge curves of PHATN in rechargeable (d) Mg and (e) Al batteries; Cycle life of PHATN in rechargeable (f) Mg and (g) Al batteries. Reproduced from reference

76 with permission from Wiley-VCH Verlag GmbH & Co. KGaA, Copyright 2018.

Apart from porous polymers, one-dimensional linear polymers have also been widely studied in organic batteries. To enhance the electrochemical performance and study the structure-performance correlation, multiple active centers and extended conjugation structures are incorporated in the repeating unit of the polymers. For example, three linear polymers (PNAI, PPAI, and PBAI) with an azo benzene moiety and an imide moiety in the repeating unit (Fig. 10a) were designed and synthesized for NIBs, KIBs, and rechargeable Al batteries.[78,79] The polymers contain the same azo benzene moiety but three different conjugated structures, a naphthalene ring, a benzene ring, and a diphenyl group in the structure units of imide moieties. All three polymers exhibited charge and discharge behaviors with redox plateaus between 1V to 3V in NIBs (Fig. 10b-d) and KIBs. However, PPAI and PBAI suffer from fast capacity decay, while PNAI delivers excellent cyclic stability upon long-term cycling (Fig. 10e), demonstrating that the extended conjugation structure (a naphthalene ring) plays a critical role in the cyclic stability of redox-active polymers. More extended conjugation structures should be designed in redox-active polymers to enhance their cycle life in rechargeable batteries. Since PNAI showed the best electrochemical performance among the three polymers, rate capability and cyclic voltammetry tests were employed to further exploit its reaction kinetics. The polymer, PNAI, showed high rate capability up to 10 A g^{-1} and surface reaction dominated kinetics, demonstrating fast-charging capability. Owing to its high performance in NIBs, it is further applied in more challenging rechargeable Al batteries. To enhance the electrochemical performance, nitrogen doped graphene is used in the polymer cathode to employ the $\pi-\pi$ stacking between conjugation structures in the graphene and the polymer (Fig. 10h). Superior electrochemical performances such as high rate capability up to 10 A g^{-1} and long cycle life up to 10,000 cycles were achieved, demonstrating that the redox-active polymer is a universal cathode material for rechargeable batteries. Therefore, these results confirm that incorporating multiple functional groups and extended conjugation structures in the polymers is an effective strategy to obtain high-performance and universal OEMs for various rechargeable batteries.

As universal electrode materials in alkali-ion, multivalent, and all-solid-state batteries, OEMs can also be used in liquid state batteries such as flow batteries. Qin et al. reported soluble polyimides for nonaqueous Mg hybrid flow batteries (Fig. 11a).[80,81] The polyimides were used as catholyte materials to couple with a Mg metal anode. Here, redox-active polymers rather than small organic molecules are used as catholyte materials in flow batteries because the large size of the polymers can mitigate the crossover of active materials through the membrane, which is a major challenge in redox-flow batteries. Carbonyl groups in the repeating unit of the polymer are redox active centers to react with Mg ions and electrons in the electrolyte, while the ether chain is employed to enhance the solubility of the polymer in the ether-based electrolyte (Fig. 11b). The ether chain length can be tuned to adjust the solubility of the polymer in the electrolyte. It was found that the polyimides with 9 to
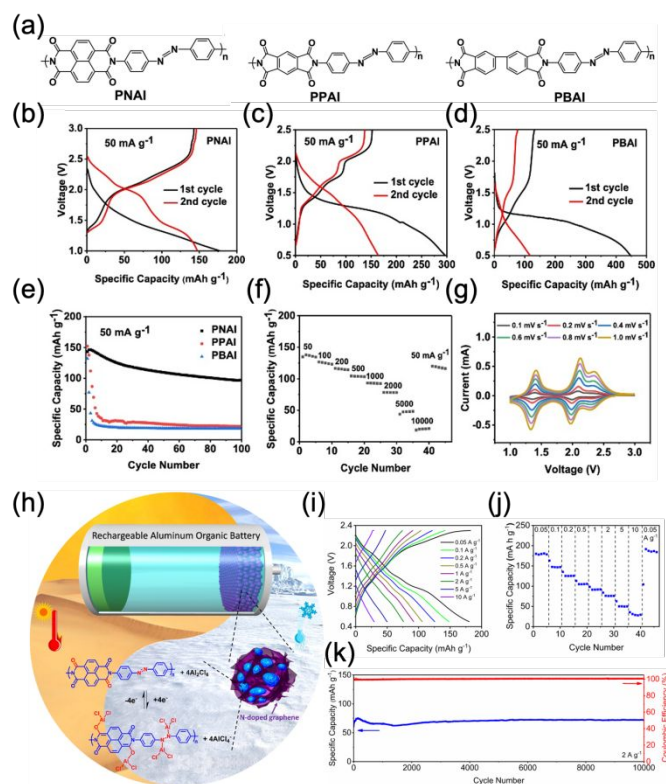

Fig. 10. Multi-functionalized polymers for Na and Al batteries. (a) The molecular structure of three multi-functionalized polymers, PNAI, PPAI, and PBAI; Galvanostatic charge-discharge curves in Na-ion batteries: (b) PNAI, (c) PPAI, (d) PBAI; (e) Charge capacity at the current density of 50 mA g^{-1} for PNAI, PPAI, and PBAI; (f) rate capability of PNAI at various current densities; (g) cyclic voltammograms of PNAI at various scan rates; Reproduced from reference 78 with permission from Wiley-VCH Verlag GmbH & Co. KGaA, Copyright 2022. (h) Schematic illustration of RAOBs; (i) Charge/discharge curves of the PNAI/NG cathode at different rates; (j) Rate performance of the PNAI/NG cathode at various current densities; (k) Discharge capacities and Coulombic efficiencies of the PNAI/NG cathode measured at 2 A g^{-1}. Reproduced from reference 79 with permission from Wiley-VCH Verlag GmbH & Co. KGaA, Copyright 2022.

11 ether groups in the repeating unit showed the highest solubility in the electrolyte. Figure 11c shows the reaction mechanism of a polyimide in flow batteries, where two carbonyl groups reversibly react with Mg ions and electrons, accompanied by intramolecular electron transfer in the conjugated structure. The reaction mechanism of polyimides in flow batteries is the same as that in the solid-state batteries, but faster kinetics is expected in flow batteries because of the molecular level distribution of organic molecules in the electrolyte. The ion diffusion in the solid particles limits reaction kinetics of solid-state batteries, but it does not exist in flow batteries. Electrochemical performances such as cyclic voltammogram, galvanostatic charge-discharge behaviors, capacity, Coulombic efficiency, voltage efficiency, and energy efficiency were shown in figure 11d, demonstrating great promise of the polyimides for flow batteries.
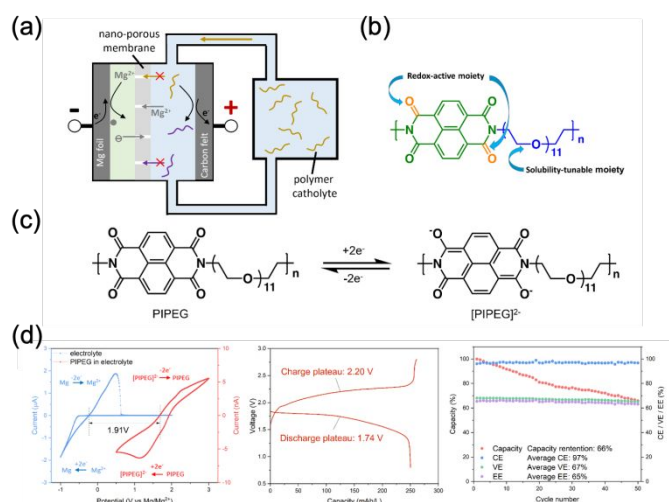
Fig. 11. Polymeric cathode materials for Mg redox-flow batteries. (a) The schematic of the Mg/polymer flow battery; (b) The structure of the polymer; (c) The reaction mechanism of the polymer during battery discharge/charge; (d) CV of the Mg anode and polymer catholyte; (e) Discharge/charge curve of the battery; (f) Cycling performance of the battery. Reproduced from reference 80 with permission from American Chemical Society, Copyright 2022.

OEMs can be used as universal electrode materials for various rechargeable batteries such as alkali ion batteries, multivalent batteries, all-solid-state batteries, redox-flow batteries, etc. Though great achievements have been made for OEMs, the performances of organic batteries are still not competitive in the commercial market due to the lack of high-performance organic/polymeric cathode materials. For organic cathode materials, including small organic compounds and redox-active polymers, their specific capacity, redox potentials, and cycle life are lower than inorganic counterparts, limiting the energy density of organic batteries. Moreover, most n-type organic/polymeric cathode materials do not provide Li ions or other cations for electrochemical reactions, so they are coupled with metal-based anodes, introducing the challenges of metal-based anodes such as uncontrollable dendrite growth and infinite volume change into organic batteries. For the p-type organic/polymeric cathode materials based on anion-insertion reactions, they deliver high redox potentials but suffer from low specific capacity. These challenges hinder the commercial applications of organic batteries.

To address these challenges and commercialize organic batteries, high structural tunability and abundant structural diversity of OEMs offer numerous opportunities for structural design and performance optimization to achieve high-performance, affordable, lightweight, and sustainable batteries. To this end, more research efforts are needed to study structure-performance correlations of OEMs in various rechargeable batteries. Though OEMs are universal electrode materials, different structural design rationales are required for different types of batteries. The different ion sizes, properties, and redox chemistries in various rechargeable batteries result in distinct challenges. Addressing the challenges for each type of batteries necessitates specific strategies. Therefore, considerable efforts should be devoted to developing new OEMs with different

molecular structures, morphologies, and interactions with other components in the electrodes to fulfill the goal of sustainable energy storage.

Mechanism Study in Organic Batteries

Organic batteries undergo various charge storage mechanisms as shown in figure 6. The redox-active functional groups, substituents, and conjugation structures are critical for charge storage in organic batteries. So far, carbonyl, imine, disulfide, azo, thiocarbonyl, and amine groups, as well as nitroxide free radicals, have been employed as active centers.[18] The substituents and conjugation structures stabilize the pristine OEMs, reaction intermediates and products, as well as accelerate reaction kinetics and tune the redox potentials. To gain insight into the mechanisms and probe the structure evolution of OEMs upon cycling, a variety of *in situ* and *ex situ* characterization techniques have been applied in the organic battery research. X-ray diffraction (XRD), Fourier-transform infrared (FTIR) spectroscopy, Raman spectroscopy, X-ray photoelectron spectroscopy (XPS), solid-state nuclear magnetic resonance (NMR), electron paramagnetic resonance (EPR), and X-ray absorption near-edge structure (XANES) spectroscopy have been used to study the reaction mechanisms of OEMs.

XRD is used to investigate the crystalline structure change of OEMs during charge and discharge. XRD patterns at various charge and discharge stages provide information about phase transition of OEMs during ion insertion and extraction. Reversibility and stability of crystalline structures upon cycling are paramount to cyclic stability of organic batteries. FTIR and Raman spectroscopies provide absorption spectra to probe the vibrations of redox-active functional groups, substituents, and conjugation structures in OEMs, offering direct evidence for the molecular structure change during charge storage. The reduction/oxidation of functional groups and rearrangement of double bonds in the conjugation structures alter the symmetric/asymmetric stretching vibrations, resulting in obvious peak shift and peak intensity change in FTIR and Raman spectra. XPS is a surface-sensitive technique to measure the binding energy between elements in OEMs. It is widely used to study the interphasial structure in batteries and can also be used to understand the charge storage mechanism in organic batteries. The redox reactions in organic batteries result in the formation of new bonds and chemical species, varying the binding energy of the elements in OEMs. The peak change in XPS spectra of each element in OEMs reflects the molecular structure evolution. Solid-state NMR is a powerful technique to study the chemical environment of elements in OEMs. The peak intensity and position change for chemical shift of the elements in OEMs demonstrate the reversible redox reactions between functional groups and charge carriers. The comparison of solid-state NMR spectra at different charge and discharge stages offers direct evidence for the charge storage mechanism. EPR is a technique to measure the presence of unpaired electrons in chemical species such as free radicals, which exist in pristine materials or reaction intermediates/products in organic batteries. The stability of unpaired electrons in pristine materials or reaction intermediates/products determines the performance of organic batteries. EPR is a unique technique to study the electron

transferring and electronic state of organic species during charge storage, providing valuable information to understand stability of reaction intermediates and reaction pathways to form the products. XANES is an analytical technique to gain insight into the local electronic structure evolution of an atom in the electrochemical process. The change of photo energy in XANES spectra shows the disappearance and formation of chemical bonds in electrochemical redox reactions, and thus is also direct evidence for the molecular structure change during charge storage. To date, there are a variety of characterization techniques to study the charge storage mechanisms of organic batteries. The combination of these techniques and computational methods are powerful to understand and confirm the charge storage mechanisms of organic batteries.

Li-S batteries

LSBs are high-energy, low-cost, lightweight, and sustainable energy storage devices due to affordability, scalability, abundance, environmental benignity, and high sustainability of sulfur resources. Coupling sulfur cathodes with lithium metal anodes endows LSBs with high energy density, which is three to five times higher than that of commercial LIBs. However, the sulfur cathode suffers from three challenges:[95,96] 1) Low conductivity of sulfur and lithium sulfides. This leads to sluggish reaction kinetics; 2) The shuttle effect of polysulfide intermediates. The high solubility of lithium polysulfides results in the loss of sulfur materials from the cathode and fast capacity fading; 3) Large volume change of sulfur-based materials during the lithiation/de-lithiation process. Large volume expansion and shrinkage of the active material upon cycling compromise the structure integrity of the sulfur cathode.

To address the challenges of sulfur cathodes, various host materials were developed to enhance the conductivity of sulfur cathodes, mitigate the shuttle effect, and accommodate the large volume change. For example, a rich variety of carbonaceous materials such as microporous and mesoporous carbon, graphene, carbon nanotubes, etc. were employed to stabilize sulfur and its reaction intermediates/product by trapping the dissolved polysulfides in the pores or carbon matrix. The high conductivity, large surface area, and porous structures of carbons also enhance the conductivity of sulfur cathodes and accommodate the large volume change from sulfur to lithium sulfide.[97] In addition to carbons, other materials such as conducting polymers and porous polymers/inorganics were also used as host materials to stabilize sulfur cathodes and improve the electrochemical performance of LSBs.[98] Apart from host materials, another strategy using high-concentration electrolytes is also used to alleviate the shuttle reactions by preventing the diffusion of dissolved polysulfides from sulfur cathodes to Li metal anodes.[99] Electrolyte engineering is critical to generate robust and stable interphases in the sulfur cathodes and Li metal anodes, which also avoid the parasitic reactions, mitigate the shuttle reactions, and accommodate the large volume change. The combination of the host materials and advanced electrolytes is an effective strategy to address the challenges of LSBs.

Besides the sulfur cathode, the lithium metal anode also suffers from two challenges:[100,101] 1) Lithium dendrite growth. Non-uniform

plating and striping of lithium metal cause the formation of lithium dendrites, which not only consume the electrolyte to continuously generate the solid-electrolyte interphase but also trigger the battery short circuit and thermal runaway; 2) Infinite volume change. Infinite volume change during the Li plating and striping process compromises structural integrity of the anode and solid-electrolyte interphase. To achieve high-performance LSBs, the challenges of both the sulfur cathode and the lithium metal anode should be addressed. Moreover, the amount of lithium metal and the liquid electrolyte should be limited for practical applications. This section briefly discusses recent progress in this field to provide guidance for the further study.
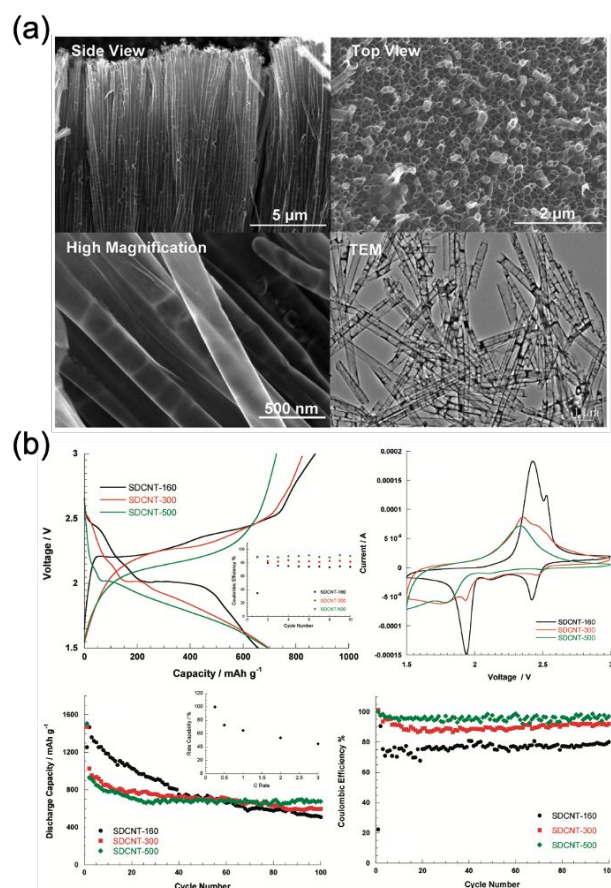

Fig. 12. (a) SEM and TEM images of the disordered carbon nanotubes; (b) Discharge/charge curves of sulfur-impregnated disordered carbon nanotubes cathodes in the second cycles and Coulombic efficiency under 10 mA g^{-1}; Cyclic voltammetry curves of the second cycles at scan rate of 0.1 mV s^{-1}; Cycling stability and Coulombic efficiencies. Reproduced from reference 102 with permission from American Chemical Society, Copyright 2011.

The carbon/small sulfur composites were reported to address the challenges of LSBs over a decade ago. Various types of carbon host materials were designed to confine small sulfur molecules in the carbon matrix by annealing the mixture of sulfur and carbon at a high temperature. Guo et al. reported disordered carbon nanotubes as host materials to stabilize small sulfur molecules.[102] The disordered carbon nanotubes, which were synthesized by a template wetting technique using commercial anodic aluminum oxide (AAO)

membranes, showed a hollow structure with a large surface area (Figure 12a). The mixture of disordered carbon nanotubes and sulfur were annealed at various temperatures from 160°C to 500°C to afford sulfur-impregnated disordered carbon nanotubes cathodes. As shown in figure 12b, different charge and discharge behaviors were obtained for these samples. For the sample prepared at 160°C, its charge and discharge behaviors are similar to that of S_8 cathodes, which generate polysulfide intermediates and trigger shuttle reactions in LSBs. However, when increasing the annealing temperatures to 300°C and 500°C, the charge and discharge behaviors of S_8 cathodes were suppressed. The average redox plateaus were lowered to ~2.1V, attributing to the S_2 to S^{2-} reaction and the strong bonding between sulfur and carbon. Improved cyclic stability was observed for the samples prepared at 300°C and 500°C due to mitigation of shuttle reactions by small sulfur molecules, carbon-sulfur bonding, and the small size (2-4 nm) of the narrow pore channel in a carbon shell.

electrolyte. Reproduced from reference 103 with permission from American Chemical Society, Copyright 2012.

To further improve the performance and form carbon/small sulfur composites, Xin et al. used a type of microporous carbon (CNT@MPC) with a narrow pore size distribution of ~0.5 nm and a large specific surface area of 936 m^2 g^{-1} to confine metastable small sulfur molecules of S_{2-4}.[103] The S/CNT@MPC sample was characterized by transmission electron microscopy (TEM), high-resolution TEM (HRTEM), annular bright-field (ABF)- scanning transmission electron microscope (STEM), and energy-dispersive X-ray (EDX) analysis. As shown in figure 13a-l, small sulfur molecules were uniformly distributed in the microporous carbon, and the sample retains good stability after 200 cycles. The galvanostatic charge and discharge curves of S/CNT@MPC (Fig. 13m) are completely different from the control sample (sulfur/carbon black, S/CB), which showed similar electrochemical behaviors as the S_8 cathode. A single output plateau at ~1.9 V was observed for S/CNT@MPC, demonstrating the redox reaction between small sulfur molecules and Li-ions/electrons. It avoids the formation of polysulfides intermedates and shuttle reactions, thus exhibits much better cyclic stability than S/CB (Fig. 13n). The high-performance of carbon/small sulfur composites demonstrates great promise for developing high-energy LSBs.
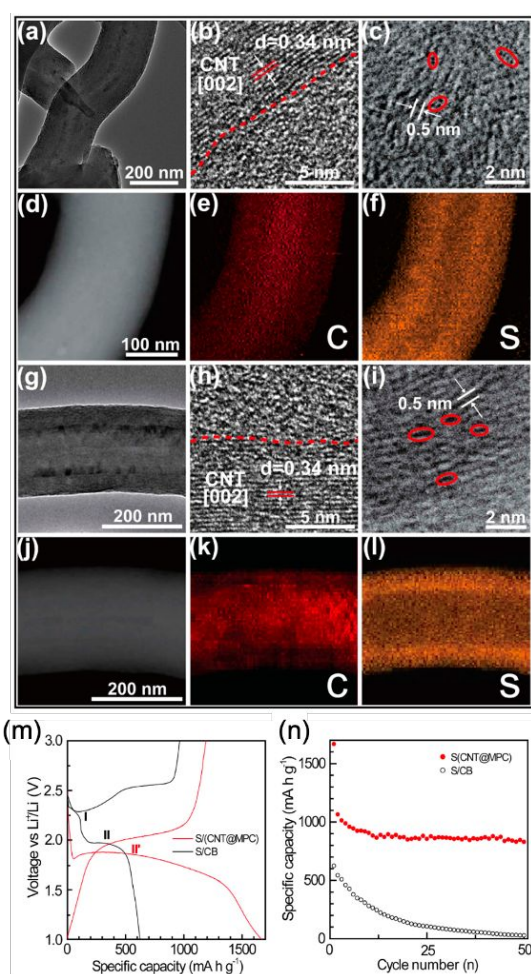

Fig. 13. Structural and electrochemical characterizations of S/(CNT@MPC). (a) TEM, (b) HRTEM, (c) ABF-STEM, (d) annular dark-field TEM, and EDX elemental mappings of (e) carbon and (f) sulfur of the S/(CNT@MPC) nanocable before cycling at 0.1C; (g) TEM, (h) HRTEM, (i) ABF-STEM, (j) annular dark-field TEM, and EDX elemental mappings of (k) carbon and (l) sulfur of the S/(CNT@MPC) nanocable after cycling at 0.1C. (m) Initial galvanostatic charge-discharge voltage profiles and (n) cycling performances in glyme-based
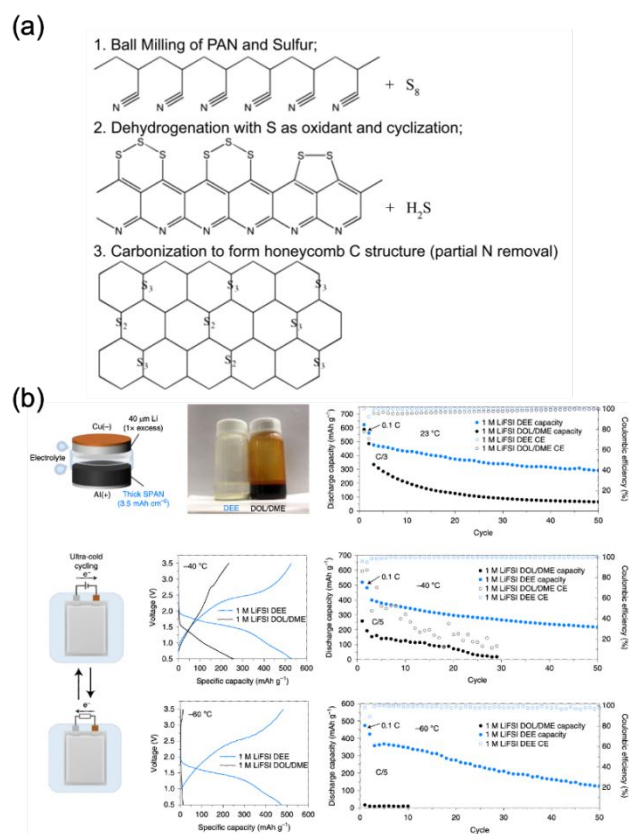

Fig. 14. (a) Proposed synthesis route for creating sulfur/polyacrylonitrile (SPAN) nanocomposite cathode materials; Reproduced from reference 104 with permission from American Chemical Society, Copyright 2015. (b) Li||SPAN full-cell performance at benign and ultra-low temperature. Reproduced from reference 105 with permission from Springer Nature, Copyright 2021.

Wei et al. proposed the synthesis route for carbon/small sulfur composites such as sulfur/polyacrylonitrile (SPAN) nanocomposite cathode materials (Fig. 14a).[104] PAN and nature sulfur (S_8) were mixed by a ball milling method, and then PAN will be dehydrogenated to form an aromatic ring structure and carbon-sulfur bonding, accompanied by H_2S gas generation during thermal treatment. Through further carbonization, covalent bonding is formed between small sulfur molecules and carbon matrix, leading to physical confinement and chemical sequestration of small sulfur species. SPAN has been widely used as a sulfur cathode material in battery research. For example, Holoubek et al. used a thick SPAN cathode to couple with a thin Li metal anode and a diethyl ether-(DEE-) based electrolyte for low-temperature battery applications.[105] The resulting Li-S pouch cells showed high performance at room temperature and low temperatures of -40°C and -60°C (Fig. 14b), demonstrating a significant step for developing high-energy batteries under extreme conditions.
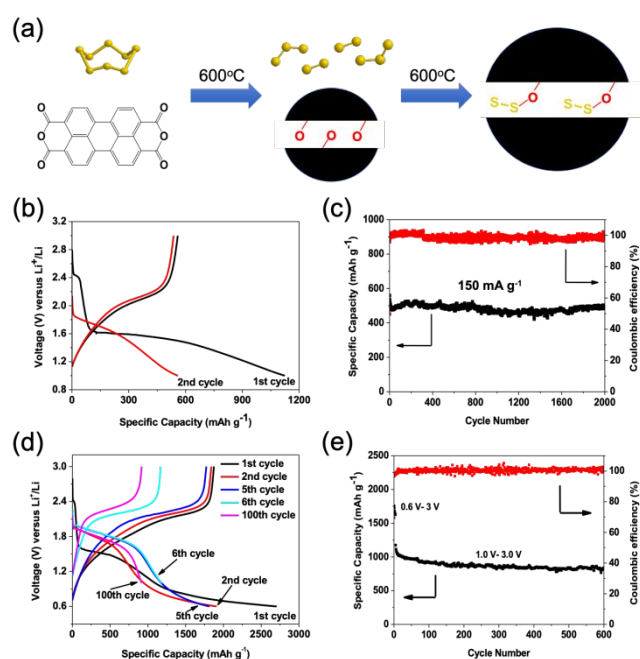

Fig. 15. Oxygen-stabilized sulfur for lithium batteries. (a) Schematic illustration for the synthetic route of the carbon/sulfur composite; (b) The galvanostatic charge–discharge curves between 1.0 and 3.0 V versus Li/Li+; (c) Delithiation capacity and Coulombic efficiency versus cycle number at the current density of 150 mA g^{-1}; (d) The galvanostatic charge–discharge curves between 0.6 and 3.0 V in initial 5 cycles and between 1.0 and 3.0 V after 5 cycles; (e) Delithiation capacity and Coulombic efficiency versus cycle number at the current density of 150 mA g^{-1} in the cutoff window from 0.6 to 3.0 V in initial 5 cycles and from 1.0 to 3.0 V after 5 cycles. (Note: the capacity is calculated based on the weight of sulfur) Reproduced from reference 106 with permission from Wiley-VCH Verlag GmbH & Co. KGaA, Copyright 2016.

As well documented, S_8 molecules can be vaporized and dissociated to small sulfur molecules such as S_2 and S_3 at the high temperature of 600°C (Fig. 15a). Small sulfur molecules can be stabilized by the carbon matrix at the room temperature. An organic

material, perylenetetracarboxylic dianhydride (PTCDA), was employed as the precursor to synthesize the oxygen-rich carbon matrix, which can form covalent bonding with small sulfur molecules to stabilize them.[106] The oxygen stabilized carbon/small sulfur composite delivered a small plateau at 2.4V corresponding to lithiation of the residual S_8 in the composite and a long plateau at 1.6V corresponding to lithiation of the small sulfur molecules during the first discharge (Fig. 15b). A reversible capacity of ~500 mAh g^{-1} based on sulfur was retained for 2,000 cycles at 150 mA g^{-1} (Fig. 15c), demonstrating high cyclic stability. However, the capacity is low in the cutoff window from 1V to 3V. To increase the reversible capacity, the oxygen stabilized carbon/small sulfur composite was discharged to 0.6V in the initial 5 cycles, and then it is cycled from 1V to 3V (Fig. 15d). After the initial activation, the reversible capacity is significantly increased to ~1,200 mAh g^{-1} in the 6th cycle and retained at 820 mAh g^{-1} after 600 cycles (Fig. 15e), demonstrating high capacity and high cyclic stability. The deep discharge to 0.6V cleavages the covalent bond between oxygen in the carbon matrix and sulfur in small sulfur molecules to release more small sulfur molecules to react with lithium ions and electrons, resulting in a higher reversible capacity. In addition, the redox plateaus centered at ~2.1V after the initial 5 cycles correspond to lithiation and de-lithiation of small sulfur molecules upon cycling. The lithiation of small sulfur molecules generates lithium sulfides directly and avoids the formation of polysulfide intermediates, preventing the shuttle effect in LSBs. Therefore, design and synthesis of carbon/small sulfur composites is an effective strategy to address the challenges in the sulfur cathode.
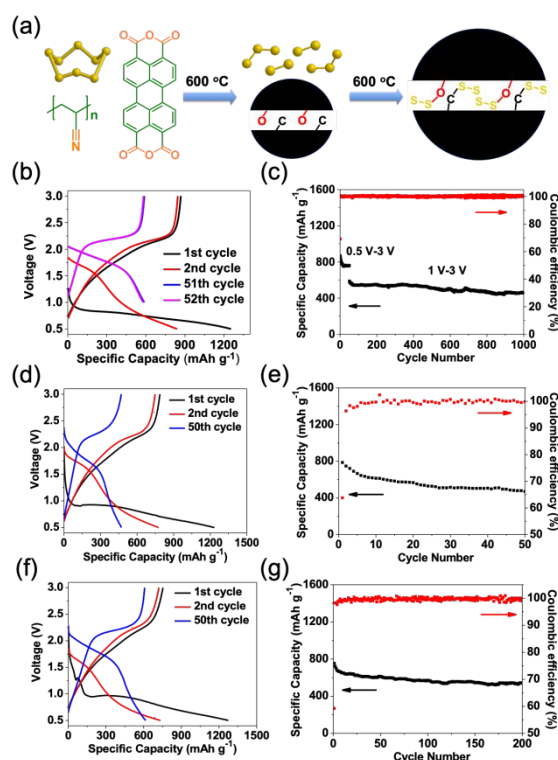

Fig. 16. A chemically stabilized sulfur cathode for LSBs.[107] (a) Schematic illustration for the synthetic route of the carbon/sulfur composite; (b) The galvanostatic charge and discharge curves at different cutoff windows at 500 mA g^{-1}; (c) Delithiation capacity and

CE versus cycle number at different cutoff windows at 500 mA g^{-1}; (d) The galvanostatic charge and discharge curves at 50 mA g^{-1} and 0.5 mA cm^{-2} in commercial 1M LiPF$_6$ in EC/DMC lean electrolyte; (e) Delithiation capacity and CE versus cycle number in commercial 1M LiPF$_6$ in EC/DMC lean electrolyte; (f) The galvanostatic charge and discharge curves at 50 mA g^{-1} and 0.5 mA cm^{-2} in all-fluorinated 1M LiPF$_6$ in FEC:FEMC:HFE lean electrolyte; (g) Delithiation capacity and CE versus cycle number in all-fluorinated 1M LiPF$_6$ in FEC:FEMC:HFE lean electrolyte. (Note: the capacity is calculated based on the weight of carbon/sulfur composites)

One of key challenges for carbon/small sulfur composites is low sulfur content (30~40 wt%) in the composites, leading to low specific capacity based on the weight of the composite. To enhance the capacity, a polymer precursor, polyacrylonitrile (PAN), was mixed with PTCDA and sulfur for the heat treatment.[107] The resulting carbon/small sulfur composite contains high sulfur content of 60 wt% by using both carbon and oxygen in the carbon matrix to bond with small sulfur molecules (Fig. 16a). After the initial activation process by deep discharging to 0.5V, the carbon/small sulfur composite delivered reversible capacity of ~600 mAh g^{-1} based on the weight of carbon/sulfur composites with a pair of redox plateaus centered at 2.1V (Fig. 16b). A long cycle life of 1,000 cycles was achieved (Fig. 16c), demonstrating excellent cyclic stability. To assess the potential for practical applications, high mass loading (10 mg cm^{-2}) and lean electrolyte (3 mL$_E$/g$_S$) conditions were applied for battery tests. An all-fluorinated 1M LiPF$_6$ in fluoroethylene carbonate/3,3,3-fluoroethylmethyl carbonate/1,1,2,2-tetrafluoroethyl-2',2',2'-trifluoroethyl ether (FEC:FEMC:HFE) electrolyte was employed, because it generates a stable and robust LiF-rich solid electrolyte interphase (SEI) on the lithium metal anode to mitigate the lithium dendrite growth and accommodate the volume change during the lithium plating and striping process. As a comparison, the commercial 1M LiPF$_6$ in EC/DMC electrolyte, which cannot form a stable SEI on the lithium metal anode, was also used. As shown in figure 16d-g, LSBs based on the carbon/small sulfur composite and the lithium metal anode can be reversibly charged and discharged under high mass loading and lean electrolyte conditions, whereas electrochemical performances in the commercial electrolyte were worse than that in the all-fluorinated electrolyte because of the stability of the lithium metal anode. The high reversible capacity can be retained for 200 cycles in the all-fluorinated lean electrolyte. These results indicate that developing advanced electrolytes for high-performance and stable lithium metal anodes is also critical for practical applications of LSBs. Considerable efforts are demanded to develop both high-capacity carbon/small sulfur composites and dendrite-free lithium metal anodes for high-energy and sustainable LSBs.

Conclusion and Outlook

Developing affordable, lightweight, and sustainable batteries such as organic batteries and LSBs is critical for the large-scale applications of energy storage devices in portable electronics, electric vehicles,

grid-scale energy storage, etc. However, the challenges in organic batteries and LSBs hinder their development and applications. To date, a rich variety of approaches and strategies have been used to address these challenges, but the performances of organic batteries and LSBs are still not competitive, compared with commercial LIBs. In organic batteries, the capacity and redox potentials of most organic cathode materials are lower than inorganic counterparts, limiting the energy density of organic batteries. Moreover, most organic cathode materials do not provide Li ions or other cations for electrochemical reactions, so they are coupled with metal-based anodes such as Li/Na/K/Mg/Al/Zn metals. This introduces the challenges of metal-based anodes such as dendrite growth and infinite volume change into organic batteries. To overcome these challenges, considerable research efforts are demanded to design and synthesize advanced OEMs with a high ratio of the number of functional groups to molecular weight for a high specific capacity, new functional groups and structures for a high redox potential, and an air-stable and cation-rich structure that can provide Li ions or other cations for electrochemical reactions.

To promote the performances and achieve rational structural design of OEMs, the study of the structure-performance correlation for OEMs in various rechargeable batteries is critical. Based on previous study on the structure-performance correlation of OEMs, some structure design rationales have been obtained. For example, the redox potential of OEMs can be enhanced or decreased by adding electron-withdrawing or electron-donating functional groups into the redox-active moieties. The extended conjugation structure in OEMs not only enhances the redox potential but also improve cyclic stability at the price of lower specific capacity. Introducing ionic bonding such as carboxylate groups in OEMs enhances the polarity and reduces the solubility in the electrolyte, resulting in improved cyclic stability. In addition, incorporating heteroatoms in the aromatic structures of OEMs can provide more active centers to enhance the specific capacity and stability. The formation of cross-linked structures and two-dimensional/three-dimensional polymers can significantly decrease the solubility of OEMs in the electrolyte and increase the electrochemical performance. To further gain insight into the structure-performance correlation and optimize the performance of OEMs, studies on the impacts of porosity and aromaticity, as well as the interfacial chemistry, are pivotal. Research efforts are demanded to develop new types of redox-active functional groups and structures based on light elements to enhance the capacity, stability, and efficiency of OEMs for practical applications.

The following research directions for organic batteries are important: (1) Developing Li-rich, air-stable, high-capacity, and high-voltage organic cathode materials for high-energy LIBs; The capacity and voltage of cathode materials limit the energy density of rechargeable batteries, so incorporating multiple functional groups into organic molecules and studying the impacts of structure isomerism, electron donating/withdrawing functional groups, and porosity to the capacity and voltage are essential to achieve high-performance organic cathodes for high-energy organic batteries. (2) Developing stable and low-cost organic cathode and anode materials for all-organic NIBs, KIBs, and dual-ion batteries; These batteries are

primarily designed for grid-scale energy storage, where the lifetime and cost of these batteries are critical. Hence, the affordability, scalability, and high stability of OEMs render them ideal candidates in these low-cost batteries. (3) Developing high-voltage and porous polymers to couple with multivalent metals (Mg/Al) for nonaqueous rechargeable multivalent metal batteries; A key challenge for multivalent batteries is sluggish reaction kinetics, caused by slow diffusivity of multivalent ions in the electrodes. Porous polymers with large surface areas and pore sizes shorten the ion diffusion pathways and accommodate the volume change, making them promising cathode materials for multivalent batteries. (4) Developing high-capacity and soft organic cathode materials for all-solid-state batteries; Soft materials can mitigate the interfacial challenge of all-solid-state batteries, enabling stable and safe all-solid-state organic batteries. (5) Developing high-capacity and high-voltage organic cathode materials for aqueous Zn metal batteries. The energy density of aqueous Zn metal batteries is lower than commercial LIBs, but it is nonflammable and more cost-effective. Therefore, aqueous Zn metal organic batteries provide another option for developing low-cost batteries.

In LSBs, the challenges for both the sulfur cathode and the lithium metal anode need to be addressed. To promote practical applications, it is critical to achieve the high sulfur mass loading and lean electrolyte LSBs. Hence, the electrolytes should not dissolve or react with any components in LSBs but only act as ion conducting medium between the cathode and the anode. To this end, developing insoluble and polysulfide-free sulfur cathodes based on carbon/small sulfur composites is an important research direction. Design and synthesis of PAN and other organic/polymeric precursors to generate carbon matrixes that can stabilize small sulfur molecules with high sulfur content of >60wt% are challenging but vital for lean electrolyte LSBs. In addition, developing advanced electrolytes that can form stable and robust SEI on the lithium metal anode to mitigate lithium dendrite growth and accommodate the infinite volume change is also a promising research direction for achieving high-energy lithium metal batteries. So far, LiF has been identified as a key component in the SEI for the stable and dendrite-free lithium metal anode, and the anion-derived SEI decomposed by contact ion pair or aggregate solvation structures in the electrolytes contains higher LiF content and is more stable, facilitating uniform lithium plating and striping. Therefore, the structures and chemistries in both the sulfur cathode and the electrolytes should be exploited to achieve high mass loading and lean electrolyte LSBs for practical applications.

To promote the commercialization of organic batteries and LSBs, the knowledge gap between laboratory research and industry manufacturing needs to be bridged. The synthetic procedures, reaction yields, material purity, and quality control are critical for materials scale-up and battery manufacturing from the lab level to the industry level. Though there are a rich variety of methods and synthetic routes to fabricate cost-effective and sustainable OEMs and carbon/sulfur composites for high-performance rechargeable batteries in the lab, the high manufacturing cost and reduced electrochemical performance under high-mass-loading and lean-electrolyte conditions in large-scale manufacturing inhibit the practical applications. To address this challenge, the material and

battery testing standard of the lab and the manufacturer should be aligned. To this end, the collaboration and communication between research labs and battery/material manufacturers are vital. The high-performance materials tested in coin cells in the lab should also be assessed in high-mass-loading pouch cells with closer testing conditions to the industrial requirement. In addition, the raw material/chemical cost, energy consumption for the synthesis, waste gas and chemical generation, the impurities in the products, and the reaction yield and purification process of each synthetic step should be considered to lower the manufacturing cost and potential risks during material synthesis. Material production should avoid the use of expensive/rare chemicals, complicated synthetic/purification procedures, and the formation of a large amount of byproducts. Apart from material manufacturing, electrode and battery manufacturing in the lab scale and industry scale is also different. It is challenging to convert the promising materials and technologies developed in the lab into industry applications. Considerable research efforts are demanded to fill the gap between the lab and the industry for the commercialization of OEMs and sulfur in affordable, lightweight, and sustainable batteries.

Due to the rapid development of smart technologies and electric transportations, the demands for affordable and sustainable energy storage devices are surging. This provides numerous opportunities for developing new battery technologies based on low-cost, abundant, and lightweight elements. Organic batteries and LSBs are such technologies, endowing next-generation energy storage with affordability, scalability, recyclability, degradability, low environmental impact, and high sustainability. The studies and applications of OEMs and sulfur in nonaqueous alkali-ion batteries, lithium metal batteries, multivalent batteries, all-solid-state batteries, dual-ion batteries, aqueous batteries, and redox-flow batteries will afford a sustainable future for the energy storage field.

Author Contributions

Dr. Chao Luo: Conceptulation, Fuding acquisition, Writing – original draft, Writing – review & editing.

Conflicts of interest

There are no conflicts to declare.

Acknowledgements

Notes and references

1   C. P. Grey and J. M. Tarascon, *Nat. Mater.*, 2016, **16**, 45–56.
2   D. Larcher and J.-M. Tarascon, *Nat. Chem.*, 2014, **7**, 19–29.
3   C. Jiang, X. Li, S. W. M. Lian, Y. Ying, J. S. Ho and J. Ping, *ACS Nano*, 2021, **15**, 9328–9354.
4   C. Xu, Y. Song, M. Han and H. Zhang, *Microsystems Nanoeng.*, 2021, **7**, 25.

5   N. Sezer and M. Koç, *Nano Energy*, 2021, **80**, 105567.
6   X. B. Cheng, R. Zhang, C. Z. Zhao and Q. Zhang, *Chem. Rev.*, 2017, **117**, 10403–10473.
7   K. Xu, *Chem. Rev.*, 2014, **114**, 11503–11618.
8   P. Poizot, J. Gaubicher, S. Renault, L. Dubois, Y. Liang and Y. Yao, *Chem. Rev.*, 2020, **120**, 6490–6557.
9   M. Li, R. P. Hicks, Z. Chen, C. Luo, J. Guo, C. Wang and Y. Xu, *Chem. Rev.*, 2023, **123**, 1712–1773.
10 Y. Lu, Q. Zhang, L. Li, Z. Niu and J. Chen, *Chem*, 2018, **4**, 2786–2813.
11 S. Muench, A. Wild, C. Friebe, B. Häupler, T. Janoschka and U. S. Schubert, *Chem. Rev.*, 2016, **116**, 9438–9484.
12 Z. Song and H. Zhou, *Energy Environ. Sci.*, 2013, **6**, 2280–2301.
13 P. G. Bruce, S. A. Freunberger, L. J. Hardwick and J. M. Tarascon, *Nat. Mater.*, 2012, **11**, 19–29.
14 A. Manthiram, Y. Fu and Y. S. Su, *Acc. Chem. Res.*, 2013, **46**, 1125–1134.
15 X. Ji, K. T. Lee and L. F. Nazar, *Nat. Mater.*, 2009, **8**, 500–506.
16 T. B. Schon, B. T. McAllister, P. F. Li and D. S. Seferos, *Chem. Soc. Rev.*, 2016, **45**, 6345–6404.
17 K. Holguin, M. Mohammadiroudbari, K. Qin and C. Luo, *J. Mater. Chem. A*, 2021, **9**, 19083–19115.
18 J. J. Shea and C. Luo, *ACS Appl. Mater. Interfaces*, 2020, **12**, 5361–5380.
19 T. Yasuda and N. Ogihara, *Chem. Commun.*, 2014, **50**, 11565–11567.
20 B. Tian, Z. Ding, G. H. Ning, W. Tang, C. Peng, B. Liu, J. Su, C. Su and K. P. Loh, *Chem. Commun.*, 2017, **53**, 2914–2917.
21 Q. Deng, C. Tian, Z. Luo, Y. Zhou, B. Gou, H. Liu, Y. Ding and R. Yang, *Chem. Commun.*, 2020, **56**, 12234–12237.
22 S. Gu, Y. Chen, R. Hao, J. Zhou, I. Hussain, N. Qin, M. Li, J. Chen, Z. Wang, W. Zheng, Q. Gan, Z. Li, H. Guo, Y. Li, K. Zhang and Z. Lu, *Chem. Commun.*, 2021, **57**, 7810–7813.
23 K. Qin, K. Holguin, M. Mohammadiroudbari and C. Luo, *Chem. Commun.*, 2021, **57**, 2360–2363.
24 S. Haldar, P. Bhauriyal, A. R. Ramuglia, A. H. Khan, S. De Kock, A. Hazra, V. Bon, D. L. Pastoetter, S. Kirchhoff, L. Shupletsov, A. De, M. A. Isaacs, X. Feng, M. Walter, E. Brunner, I. M. Weidinger, T. Heine, A. Schneemann and S. Kaskel, *Adv. Mater.*, 2023, 2210151.
25 H. Wang, B. D. Adams, H. Pan, L. Zhang, K. S. Han, L. Estevez, D. Lu, H. Jia, J. Feng, J. Guo, K. R. Zavadil, Y. Shao and J. G. Zhang, *Adv. Energy Mater.*, 2018, **8**, 1800590.
26 S. Wei, L. Ma, K. E. Hendrickson, Z. Tu and L. A. Archer, *J. Am. Chem. Soc.*, 2015, **137**, 12143–12152.
27 Z. Li, J. Zhang, Y. Lu and X. W. Lou, *Sci. Adv.*, 2018, **4**, eaat1687.
28 H. O. Ford, P. He and J. L. Schaefer, *ChemPhysChem*, 2022, **23**, e202100881.
29 H. O. Ford, E. S. Doyle, P. He, W. C. Boggess, A. G. Oliver, T. Wu, G. E. Sterbinsky and J. L. Schaefer, *Energy Environ. Sci.*, 2021, **14**, 890–899.
30 B. Ding, J. Wang, Z. Fan, S. Chen, Q. Lin, X. Lu, H. Dou, A. Kumar Nanjundan, G. Yushin, X. Zhang and Y. Yamauchi, *Mater. Today*, 2020, **40**, 114–131.
31 X. Dong, Z. Guo, Z. Guo, Y. Wang and Y. Xia, *Joule*, 2018, **2**, 902–913.
32 C. Han, J. Zhu, C. Zhi and H. Li, *J. Mater. Chem. A*, 2020, **8**, 15479–15512.
33 Z. Song, T. Xu, M. L. Gordin, Y. B. Jiang, I. T. Bae, Q. Xiao, H. Zhan, J. Liu and D. Wang, *Nano Lett.*, 2012, **12**, 2205–2211.
34 X. Lu, X. Pan, D. Zhang, Z. Fang, S. Xu, Y. Ma, Q. Liu, G. Shao, D. Fu, J. Teng and W. Yang, *Proc. Natl. Acad. Sci. U. S. A.*, 2021, **118**, e2110912118.
35 J. Holoubek, H. Liu, Z. Wu, Y. Yin, X. Xing, G. Cai, S. Yu, H. Zhou, T. A. Pascal, Z. Chen and P. Liu, *Nat. Energy*, 2021, **6**, 303–313.
36 J. K. Kim, Y. Kim, S. Park, H. Ko and Y. Kim, *Energy Environ. Sci.*, 2016, **9**, 1264–1269.

37 Z. Jin, Q. Cheng, A. M. Evans, J. Gray, R. Zhang, S. T. Bao, F. Wei, L. Venkataraman, Y. Yang and C. Nuckolls, *Chem. Sci.*, 2022, **13**, 3533–3538.
38 Y. Ham, N. J. Fritz, G. Hyun, Y. B. Lee, J. S. Nam, I. D. Kim, P. V. Braun and S. Jeon, *Energy Environ. Sci.*, 2021, **14**, 5894–5902.
39 H. Zhang, Y. Geng, J. Huang, Z. Wang, K. Du and H. Li, *Energy Environ. Sci.*, 2023, **16**, 889–951.
40 X. Fan, F. Wang, X. Ji, R. Wang, T. Gao, S. Hou, J. Chen, T. Deng, X. Li, L. Chen, C. Luo, L. Wang and C. Wang, *Angew. Chemie - Int. Ed.*, 2018, **57**, 7146–7150.
41 Y. Lu, X. Hou, L. Miao, L. Li, R. Shi, L. Liu and J. Chen, *Angew. Chemie - Int. Ed.*, 2019, **58**, 7020–7024.
42 M. Yao, H. Senoh, S. I. Yamazaki, Z. Siroma, T. Sakai and K. Yasuda, *J. Power Sources*, 2010, **195**, 8336–8340.
43 M. Mohammadiroudbari, J. Huang, E.Y. Kim, Z. Yang, F. Chen and C. Luo, *J. Mater. Chem. A*, 2023, DOI: 10.1039/D3TA02445H.
44 J. Wang, A. E. Lakraychi, X. Liu, L. Sieuw, C. Morari, P. Poizot and A. Vlad, *Nat. Mater.*, 2021, **20**, 665–673.
45 S. Feng, R. K. Singh, Y. Fu, Z. Li, Y. Wang, J. Bao, Z. Xu, G. Li, C. Anderson, L. Shi, Y. Lin, P. G. Khalifah, W. Wang, J. Liu, J. Xiao and D. Lu, *Energy Environ. Sci.*, 2022, **15**, 3842–3853.
46 H. Wang, Y. Yang, Y. Liang, J. T. Robinson, Y. Li and A. Jackson, Y. Cui and H. Dai, *Nano Lett.*, 2011, **11**, 2644–2647.
47 J. Chen, W. A. Henderson, H. Pan, B. R. Perdue, R. Cao, J. Z. Hu, C. Wan, K. S. Han, K. T. Mueller, J. G. Zhang, Y. Shao and J. Liu, *Nano Lett.*, 2017, **17**, 3061–3067.
48 G. Li, W. Lei, D. Luo, Y. Deng, Z. Deng, D. Wang, A. Yu and Z. Chen, *Energy Environ. Sci.*, 2018, **11**, 2372–2381.
49 H. Pan, K. S. Han, M. H. Engelhard, R. Cao, J. Chen, J. G. Zhang, K. T. Mueller, Y. Shao and J. Liu, *Adv. Funct. Mater.*, 2018, **28**, 1707234.
50 J. K. Kim, *J. Power Sources*, 2020, **477**, 228670.
51 K. Sakaushi, E. Hosono, G. Nickerl, T. Gemming, H. Zhou, S. Kaskel and J. Eckert, *Nat. Commun.*, 2013, **4**, 1485.
52 X. Chen, H. Zhang, C. Ci, W. Sun and Y. Wang, *ACS Nano*, 2019, **13**, 3600–3607.
53 S. Zhang, W. Huang, P. Hu, C. Huang, C. Shang, C. Zhang, R. Yang and G. Cui, *J. Mater. Chem. A*, 2015, **3**, 1896–1901.
54 B. Häupler, A. Wild and U. S. Schubert, *Adv. Energy Mater.*, 2015, **5**, 1402034.
55 Z. J. Zheng, H. Ye and Z. P. Guo, *Energy Environ. Sci.*, 2021, **14**, 1835–1853.
56 N. Jayaprakash, J. Shen, S. S. Moganty, A. Corona and L. A. Archer, *Angew. Chemie - Int. Ed.*, 2011, **50**, 5904–5908.
57 Z. W. Seh, W. Li, J. J. Cha, G. Zheng, Y. Yang, M. T. McDowell, P. C. Hsu and Y. Cui, *Nat. Commun.*, 2013, **4**, 1331.
58 L. Suo, Y. S. Hu, H. Li, M. Armand and L. Chen, *Nat. Commun.*, 2013, **4**, 1481.
59 J. Schuster, G. He, B. Mandlmeier, T. Yim, K. T. Lee, T. Bein and L. F. Nazar, Angew. Chemie - Int. Ed., 2012, 51, 3591–3595.
60 K. Qin, J. Huang, K. Holguin and C. Luo, *Energy Environ. Sci.*, 2020, **13**, 3950–3992.
61 Y. Liang, Z. Tao and J. Chen, *Adv. Energy Mater.*, 2012, **2**, 742–769.
62 C. Luo, R. Huang, R. Kevorkyants, M. Pavanello, H. He and C. Wang, *Nano Lett.*, 2014, **14**, 1596–1602.
63 C. Luo, Y. Zhu, Y. Xu, Y. Liu, T. Gao, J. Wang and C. Wang, *J. Power Sources*, 2014, **250**, 372–378.
64 C. Luo, J. Wang, X. Fan, Y. Zhu, F. Han, L. Suo and C. Wang, *Nano Energy*, 2015, **13**, 537–545.
65 C. Luo, X. Fan, Z. Ma, T. Gao and C. Wang, *Chem*, 2017, **3**, 1050–1062.
66 C. Luo, J. J. Shea and J. Huang, *J. Power Sources*, 2020, **453**, 227904.
67 C. Cui, X. Ji, P. F. Wang, G. L. Xu, L. Chen, J. Chen, H. Kim, Y. Ren, F. Chen, C. Yang, X. Fan, C. Luo, K. Amine and C. Wang, *ACS Energy Lett.*, 2020, **5**, 224–231.

68 J. Huang, K. I. E. Callender, K. Qin, M. Girgis, M. Paige, Z. Yang, A. Z. Clayborne and C. Luo, *ACS Appl. Mater. Interfaces*, 2022, **14**, 40784–40792.

69 K. Holguin, K. Qin, E. P. Kamphaus, F. Chen, L. Cheng, G.-L. Xu, K. Amine and C. Luo, *J. Power Sources*, 2022, **533**, 231383.

70 K. Holguin, K. Qin, J. Huang and C. Luo, *New J. Chem.*, 2022, 18890–18898.

71 C. Luo, O. Borodin, X. Ji, S. Hou, K. J. Gaskell, X. Fan, J. Chen, T. Deng, R. Wang, J. Jiang and C. Wang, *Proc. Natl. Acad. Sci. U. S. A.*, 2018, **115**, 2004–2009.

72 C. Luo, G. L. Xu, X. Ji, S. Hou, L. Chen, F. Wang, J. Jiang, Z. Chen, Y. Ren, K. Amine and C. Wang, *Angew. Chemie - Int. Ed.*, 2018, **57**, 2879–2883.

73 Y. Liang, C. Luo, F. Wang, S. Hou, S.-C. Liou, T. Qing, Q. Li, J. Zheng, C. Cui and C. Wang, *Adv. Energy Mater.*, 2018, **9**, 1802986.

74 C. Luo, X. Ji, J. Chen, K. J. Gaskell, X. He, Y. Liang, J. Jiang and C. Wang, *Angew. Chemie - Int. Ed.*, 2018, **57**, 8567–8571.

75 C. Luo, X. Ji, S. Hou, N. Eidson, X. Fan, Y. Liang, T. Deng, J. Jiang and C. Wang, *Adv. Mater.*, 2018, **30**, 1706498.

76 M. Mao, C. Luo, T. P. Pollard, S. Hou, T. Gao, X. Fan, C. Cui, J. Yue, Y. Tong, G. Yang, T. Deng, M. Zhang, J. Ma, L. Suo, O. Borodin and C. Wang, *Angew. Chemie - Int. Ed.*, 2019, **58**, 17820–17826.

77 R. Sun, S. Hou, C. Luo, X. Ji, L. Wang, L. Mai and C. Wang, *Nano Lett.*, 2020, **20**, 3880–3888.

78 M. Mohammadiroudbari, K. Qin and C. Luo, *Batter. Supercaps*, 2022, **5**, e202200021.

79 K. Qin, S. Tan, M. Mohammadiroudbari, Z. Yang, X. Q. Yang, E. Hu and C. Luo, *Nano Energy*, 2022, **101**, 107554.

80 Y. Qin, K. Holguin, D. Fehlau, C. Luo and T. Gao, *ACS Appl. Energy Mater.*, 2022, **5**, 2675–2678.

81 Y. Qin, K. Holguin, D. Fehlau, C. Luo and T. Gao, *Chem. - An Asian J.*, 2022, **17**, e202200587.

82 J. Song, M. L. Gordin, T. Xu, S. Chen, Z. Yu, H. Sohn, J. Lu, Y. Ren, Y. Duan and D. Wang, *Angew. Chemie - Int. Ed.*, 2015, **54**, 4325–4329.

83 W. Zhou, C. Wang, Q. Zhang, H. D. Abruña, Y. He, J. Wang, S. X. Mao and X. Xiao, *Adv. Energy Mater.*, 2015, **5**, 1401752.

84 W. Xue, Z. Shi, L. Suo, C. Wang, Z. Wang, H. Wang, K. P. So, A. Maurano, D. Yu, Y. Chen, L. Qie, Z. Zhu, G. Xu, J. Kong and J. Li, *Nat. Energy*, 2019, **4**, 374–382.

85 X. Zhao, C. Wang, Z. Li, X. Hu, A. Abdul Razzaq and Z. Deng, *J. Mater. Chem. A*, 2021, **9**, 19282–19297.

86 C. Luo, Y. Xu, Y. Zhu, Y. Liu, S. Zheng, Y. Liu, A. Langrock and C. Wang, *ACS Nano*, 2013, **7**, 8003–8010.

87 C. Luo, J. Wang, L. Suo, J. Mao, X. Fan and C. Wang, *J. Mater. Chem. A*, 2015, **3**, 555–561.

88 C. Luo, Y. Zhu, Y. Wen, J. Wang and C. Wang, *Adv. Funct. Mater.*, **24**, 4082–4089.

89 C. Luo, H. Zhu, W. Luo, F. Shen, X. Fan, J. Dai, Y. Liang, C. Wang and L. Hu, *ACS Appl. Mater. Interfaces*, 2017, **9**, 14801–14807.

90 K. Qin, K. Holguin, M. Mohammadiroudbari, J. Huang, E. Y. S. Kim, R. Hall and C. Luo, *Adv. Funct. Mater.* 2021, **31**, 2009694.

91 C. Jia, A. Duan, C. Liu, W. Wang, S. Gan, Q. Qi, Y. Li, X. Huang and X. Zhao, Small, 2023, 2300518.

92 C. Wang, *Energy Environ. Mater.*, 2020, **3**, 441–452.

93 C. Zhang, Y. Qiao, P. Xiong, W. Ma, P. Bai, X. Wang, Q. Li, J. Zhao, Y. Xu, Y. Chen, J. H. Zeng, F. Wang, Y. Xu and J. X. Jiang, *ACS Nano*, 2019, **13**, 745–754.

94 K. Qin, K. Holguin, J. Huang, M. Mohammadiroudbari, F. Chen, Z. Yang, G. L. Xu and C. Luo, *Adv. Sci.*, 2022, **9**, 2106116.

95 S. Tu, X. Chen, X. Zhao, M. Cheng, P. Xiong, Y. He, Q. Zhang and Y. Xu, *Adv. Mater.*, 2018, **30**, 1804581.

96 P. Xiong, X. Han, X. Zhao, P. Bai, Y. Liu, J. Sun and Y. Xu, *ACS Nano*, 2019, **13**, 2536–2543.

97 H. Yuan, T. Liu, Y. Liu, J. Nai, Y. Wang, W. Zhang and X. Tao, *Chem. Sci.*, 2019, **10**, 7484–7495.

98 B. J. Lee, C. Zhao, J. H. Yu, T. H. Kang, H. Y. Park, J. Kang, Y. Jung, X. Liu, T. Li, W. Xu, X. B. Zuo, G. L. Xu, K. Amine and J. S. Yu, *Nat. Commun.*, 2022, **13**, 4629.

99 L. Suo, Y. S. Hu, H. Li, M. Armand and L. Chen, *Nat. Commun.*, 2013, **4**, 1481.

100 X. Fan, L. Chen, O. Borodin, X. Ji, J. Chen, S. Hou, T. Deng, J. Zheng, C. Yang, S. C. Liou, K. Amine, K. Xu and C. Wang, *Nat. Nanotechnol.*, 2018, **13**, 715–722.

101 L. Li, S. Basu, Y. Wang, Z. Chen, P. Hundekar, B. Wang, J. Shi, Y. Shi, S. Narayanan and N. Koratkar, *Science*, 2018, **359**, 1513–1516.

102 J. Guo, Y. Xu and C. Wang, *Nano Lett.*, 2011, **11**, 4288–4294.

103 S. Xin, L. Gu, N. H. Zhao, Y. X. Yin, L. J. Zhou, Y. G. Guo and L. J. Wan, *J. Am. Chem. Soc.*, 2012, **134**, 18510–18513.

104 S. Wei, L. Ma, K. E. Hendrickson, Z. Tu and L. A. Archer, *J. Am. Chem. Soc.*, 2015, **137**, 12143–12152.

105 J. Holoubek, H. Liu, Z. Wu, Y. Yin, X. Xing, G. Cai, S. Yu, H. Zhou, T. A. Pascal, Z. Chen and P. Liu, *Nat. Energy*, 2021, **6**, 303–313.

106 C. Luo, Y. Zhu, O. Borodin, T. Gao, X. Fan, Y. Xu, K. Xu and C. Wang, *Adv. Funct. Mater.*, 2016, **26**, 745–752.

107 C. Luo, E. Hu, K. J. Gaskell, X. Fan, T. Gao, C. Cui, S. Ghose, X. Q. Yang and C. Wang, *Proc. Natl. Acad. Sci. U. S. A.*, 2020, **117**, 14712–14720.